Nano-Bio-Imaging

DOI: 10.1002/ange.201203728

Tracking Bisphosphonates through a 20 mm Thick Porcine Tissue by Using Surface-Enhanced Spatially Offset Raman Spectroscopy**

*Hai-nan Xie, Ross Stevenson, Nicholas Stone, Aaron Hernandez-Santana, Karen Faulds, and Duncan Graham**

Bisphosphonates (BPs) are an important class of drugs used in the treatment of osteoporosis and other conditions involving bone fragility.[1] Tumor cells in the bone-marrow cavity secrete a variety of paracrine factors that stimulate bone formation and the stimulation of osteoclast function is of key importance.[2] This results in osteolysis, which is typically associated with disruption of the normal coupling signals that control the relative levels of osteoblast and osteoclast function. It is in this situation that bisphosphonates are able to offer their therapeutic potential in skeletal metastatic disease.[2] To monitor the progress of the disease and the effectiveness of therapy, it is vital to identify the bisphosphonate localization in treatments. Recently, a number of approaches have exploited the specificity of bisphosphonates to create bone-imaging reagents,[3] such as NIR-bisphosphonate dyes[4] and ^{99m}Tc labeled bisphosphonates.[5] Their success as therapeutic drugs and bone-imaging agents relies on their exceptional selectivity and strong affinity for solid-phase calcium hydroxyapatite which is predominantly found in bones.[6] Hernandez-Santana et al. isolated calcium phosphate crystals from complex biological fluids using bisphosphonate-modified superparamagnetic beads.[7] However, this work focused only on the isolation of the calcium phosphate crystals and lack of subsequent detection limited its further applications.

Surface-enhanced Raman scattering (SERS) provides a non-invasive molecular detection that can be tuned to the near infrared (NIR) region, which is of significant biological importance as this region provides a clear spectral window for both therapeutic and imaging applications in tissue.[8] However, the depth of penetration (less than 10 mm) remains an obstacle for most in vivo SERS applications.[9] An alternative approach is to use spatially offset Raman spectroscopy (SORS) which relies on moving the area of collection of the scattered light away from the laser-illuminated zone and allows highly accurate chemical analysis of objects beneath obscuring surfaces, such as tissue, coatings, and bottles.[10] Preliminary results from our group in collaboration with Stone and Matousek[11] allowed a recognizable signal from SERS active nanoparticles (NPs) at a depth of around 50 mm in tissues to be obtained. Subsequent work by Van Duyne and co-workers on the subcutaneous detection of glucose also shows the great promise of SORS in biological applications.[12]

Herein, we used porcine bones, consisting mainly of calcium hydroxyapatite and bisphosphonate-functionalized SERS nanotags as Raman reporters for a simulation study of tracking the bisphosphonate localization through SERS which could be useful both in metastatic breast cancer and bone disease treatments. To demonstrate the in vivo application potential, bone fragments pre-incubated with functionalized nanotags were inserted into 20 mm thick specimens of porcine muscle tissue allowing observation of Raman through surface-enhanced spatially offset Raman spectroscopy (SESORS). Unlike previous work,[11b] a fine distribution of nanotags on the surface of the bone was measured rather than a concentrated droplet injected into the tissue. We believe our work is the first bone/calcium hydroxyapatite-specific tag detectable by SERS/SESORS. It provides great potential for non-invasive in vivo tracking of the bisphosphonate localization in treatment for metastatic breast cancer and bone disease.

Commercially available SERS nanotags were functionalized with bisphosphonate (Neridronate), which can provide specific binding to calcium phosphate salts, to provide a SERS specific identification of bisphosphonate localization.

Figure 1 a illustrates the functionalization of encapsulated SERS active thiol-modified nanoparticles through sulfosuccinimidyl-4-(*N*-maleimidomethyl)cyclohexane-1-carboxylate (sulfo-SMCC) couplings.[13] Bisphosphonate and sulfo-SMCC were replaced with buffer solution in the three different controls to confirm that binding of bisphosphonate-functionalized nanotags to the surface of bones only occurred in positive samples. Bone fragments were placed in the different nanotag solutions, gently shaken overnight and washed with water followed by sonication. Raman spectra of bisphosphonate-functionalized nanotag covered bones and blank bones are shown in Figure 1 b. The solution SERS spectrum of nanotags is also given as a reference. The bone surface is not completely flat making it difficult to perform Raman maps because of issues with focusing the laser beam onto the rough surface. To minimize this problem, but still gain enough signals, a 20× objective lens was used and the mapping geometry was confined to 50 μm × 50 μm. The peak at around 960 cm^{-1} observed in both samples arose from the phosphate

[*] H. Xie, Dr. R. Stevenson, Dr. A. Hernandez-Santana, Dr. K. Faulds, Prof. D. Graham
Centre for Molecular Nanometrology, WestCHEM
Department of Pure and Applied Chemistry
University of Strathclyde
295 Cathedral Street, Glasgow, G1 1XL (UK)
E-mail: duncan.graham@strath.ac.uk
Prof. N. Stone
Biophotonics Research Unit, Gloucestershire Hospitals NHS Foundation Trust (UK)

[**] We thank Prof. Michael Natan, Cabot Security Materials Inc for provision of the nanotags used in this study.

Supporting information for this article is available on the WWW under http://dx.doi.org/10.1002/anie.201203728.

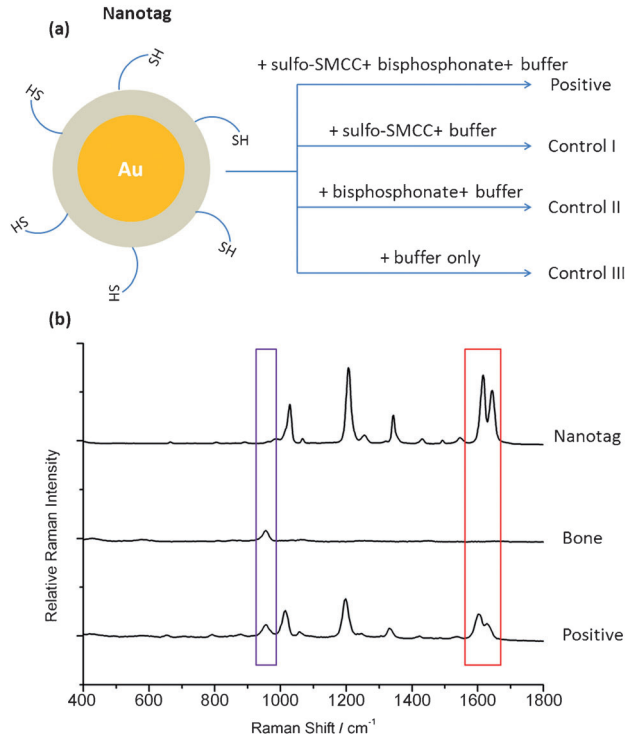

Figure 1. a) Schematic illustration of the bisphosphonate functionalization of nanotags. b) Raman spectra of nanotag only, bone only, and positive (i.e. bisphosphonate-functionalized nanotag covered bones) samples. The peak at around 960 cm^{-1} (purple box) arising from the phosphate stretch in bone was observed in the positive and bone samples only and was used as an internal reference. One of the nanotag characteristic peaks (at around 1600 cm^{-1}; red box) was chosen as the monitored peak in the subsequent maps.

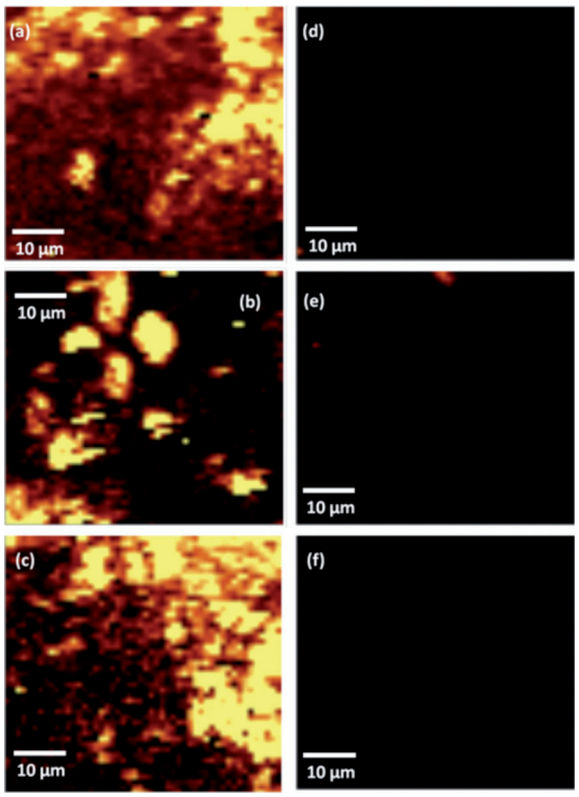

Figure 2. SERS maps of different bone samples using the same false-color scale. Bright yellow indicates the highest SERS intensity and black indicates the lowest intensity. a), b) and c) are different pieces of bisphonsphonate-functionalized nanotag (positive) covered bones; d) control I; e) control II; f) control III.

stretch of the bone.[14] This peak was used as an internal reference throughout, thus ensuring the absence of nanotag signal was not because of poor objective focusing.

False-color SERS maps were constructed using the intensity of the monitored peak of the nanotag (around 1600 cm^{-1}). Three different bone pieces, which were bound to bisphosphonate functionalized nanotags, show very different images compared to the control samples as can be seen in Figure 2. This difference is due to the chelation of the bisphosphonic moiety with superficial Ca^{2+} ions on the bone surface. The spectra within each pixel of the maps were also checked to ensure that the phosphate stretch from the bone could also be observed, especially for the controls where no nanotag SERS spectrum would be expected, thus ensuring that a signal was being observed from the surface of the bone and the laser was correctly focused on the surface. Despite Figures 2 d and 2e showing some very weak signals because of the non-specific adsorption of a small amount of nanotags, no obvious spots were observed in the control samples. Bone samples were sonicated in water to reduce the non-specific binding, however we assume that nanotags could still be trapped inside the cavities on the bone surface. Nevertheless, a huge discrimination between positive samples and controls were observed. To ensure reproducible results, another two different bone fragments were covered by bisphosphonate-functionalized nanotags and the SERS maps were also performed in three different areas of each bone fragment. These SERS maps of positive and control bone samples are shown in Figure S1 and S2 of the Supporting Information and the same discrimination between positive and control samples was observed. Therefore, the bisphosphonate-functionalized nanotags show strongly specific binding to the bone surface (calcium hydroxyapatite).

To mimic the applications of these nanotags in vivo, bisphosphonate-functionalized nanotag covered bone was inserted into a 20 mm thick specimen of porcine muscle tissue to simulate the detection of the nanotag functionalized bone through tissue in the case of detecting skeletal metastases (Figure S3). Spatially offset Raman maps were performed across the bone with 2 mm steps 0–20 mm in the x direction and 0–10 mm in the y direction.

The SESORS map shown in Figure 3 was constructed by calculating the principal components of the spectral data set and selecting the one most appropriate to represent the nanoparticle signal from the bone. The second principle component (PC2), which represented the nanoparticle signal from the buried bone, was selected and the loading vector and the scores map is shown in Figure 3, alongside the raw spectrum from the nanotags. The most intense nanotag peak can be seen at around 1200 cm^{-1}; the 960 cm^{-1} signal from the hydroxyapatite is also visible and clearly correlated with the nanoparticle signal. Unlike previous experiments,[11b] a fine

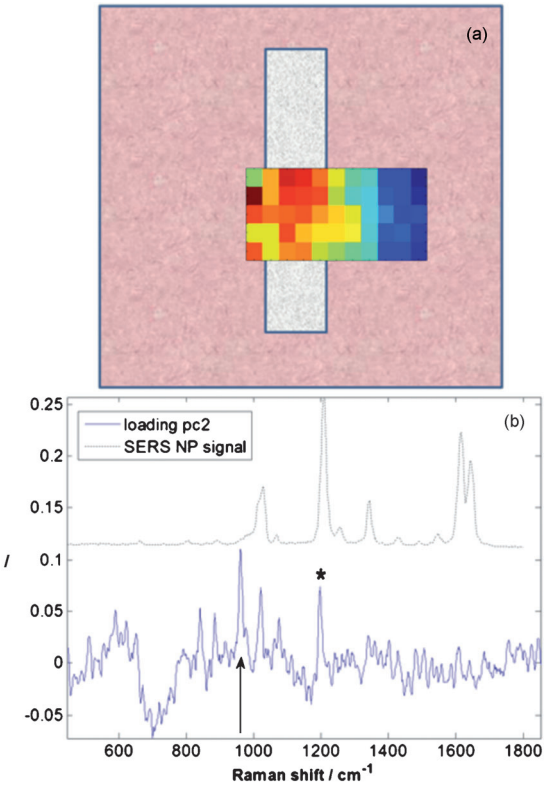

Figure 3. False-color SESORS map of nanotag-covered bone inserted into a 20 mm thick porcine tissue. a) The gray box represents the bone (ca. 8 mm across (*x* dimension) corresponding to four pixels in the false-color image). b) The nanotag characteristic peaks are highlighted in the top spectral plot and the principal component loading plot (bottom) shows the characteristic nanoparticle signal (*) and the hydroxyapatite signal from the bone at 960 cm^{-1} (arrow). The false-color image demonstrates the distribution of the signals as described by PC2.

distribution of NPs on the surface of the bone was measured rather than a concentrated droplet injected into the tissue. A significant signal reduction particularly above 1250 cm^{-1} was observed through a 20 mm thick tissue when compared to the previous SERS maps carried out on the bone surface directly. Two reasons are proposed: first, at these wavelengths both water and myoglobin contribute to the absorption. The 1250 to 1600 cm^{-1} Stokes-shifted range with a 830 nm excitation equals to around 925 to 957 nm, which covers the range where a strong lipid absorption band (ca. 930 nm)[15] and water absorption band (max ca. 970 nm)[16] are located. In addition, a more subtle contribution also comes from a rising absorption in this wavelength region from myoglobin.[17]

In summary, we used porcine bones, containing calcium hydroxyapatite and bisphosphonate-functionalized nanotags as Raman reporters for a simulation study of tracking the bisphosphonate localization through SERS which could be useful both in metastatic breast cancer and bone disease treatments. Functionalized nanotags (positive) specifically bind to bone through the optimized chelation of the bisphosphonic moiety with superficial Ca^{2+} ions on the bone surface. A recognized nanotag signal was gained from a fine distribution of nanotags on the surface of the bone when placed in a 20 mm thick specimen of porcine muscle tissue through surface-enhanced spatially offset Raman spectroscopy (SESORS) demonstrating the great potential for non-invasive in vivo bisphosphonate tracking. This work is the first bone/calcium hydroxyapatite-specific tag detectable by SERS/SESORS. In the future, we plan to work on the in vitro (osteoblasts) and in vivo applications of bisphosphonate functionalized nanotags through SERS.

Received: May 14, 2012
Published online: July 4, 2012

Keywords: bisphosphonates · cancer · nanotags · Raman spectroscopy · SERS

[1] J. Catterall, T. Cawston, *Arthritis Res. Ther.* **2003**, *5*, 12–24.
[2] J. Brown, R. Coleman, *Breast Cancer Res.* **2002**, *4*, 24–29.
[3] S. Zhang, G. Gangal, H. Uludag, *Chem. Soc. Rev.* **2007**, *36*, 507–531.
[4] A. Zaheer, R. E. Lenkinski, A. Mahmood, A. G. Jones, L. C. Cantley, J. V. Frangioni, *Nat. Biotechnol.* **2001**, *19*, 1148–1154.
[5] K. Wang, L. Allen, E. Fung, C. C. Chan, J. C. S. Chan, J. F. Griffith, *Clin. Nucl. Med.* **2005**, *30*, 655–671.
[6] M. R. Christoffersen, J. Christoffersen, *Cryst. Growth Des.* **2003**, *3*, 79–82.
[7] A. Hernandez-Santana, A. Yavorskyy, A. Olinyole, G. M. McCarthy, G. P. McMahon, *Chem. Commun.* **2008**, 2686–2688.
[8] a) A. M. Gobin, M. H. Lee, N. J. Halas, W. D. James, R. A. Drezek, J. L. West, *Nano Lett.* **2007**, *7*, 1929–1934; b) R. Weissleder, *Nat. Biotechnol.* **2001**, *19*, 316–317.
[9] I. A. Larmour, D. Graham, *Analyst* **2011**, *136*, 3831–3853.
[10] a) N. Stone, R. Baker, K. Rogers, A. W. Parker, P. Matousek, *Analyst* **2007**, *132*, 899–905; b) P. Matousek, I. P. Clark, E. R. C. Draper, M. D. Morris, A. E. Goodship, N. Everall, M. Towrie, W. F. Finney, A. W. Parker, *Appl. Spectrosc.* **2005**, *59*, 393–400; c) P. Matousek, M. D. Morris, N. Everall, I. P. Clark, M. Towrie, E. Draper, A. Goodship, A. W. Parker, *Appl. Spectrosc.* **2005**, *59*, 1485–1492.
[11] a) N. Stone, K. Faulds, D. Graham, P. Matousek, *Anal. Chem.* **2010**, *82*, 3969–3973; b) N. Stone, M. Kerssens, G. R. Lloyd, K. Faulds, D. Graham, P. Matousek, *Chem. Sci.* **2011**, *2*, 776–780.
[12] a) J. M. Yuen, N. C. Shah, J. T. Walsh, M. R. Glucksberg, R. P. Van Duyne, *Anal. Chem.* **2010**, *82*, 8382–8385; b) K. Ma, J. M. Yuen, N. C. Shah, J. T. Walsh, M. R. Glucksberg, R. P. Van Duyne, *Anal. Chem.* **2011**, *83*, 9146–9152.
[13] L. Muller, M. D. de Escauriaza, P. Lajoie, M. Theis, M. Jung, A. Muller, C. Burgard, M. Greiner, E. L. Snapp, J. Dudek, R. Zimmermann, *Mol. Biol. Cell* **2010**, *21*, 691–703.
[14] J. Timlin, *J. Biomed. Opt.* **1999**, *4*, 28.
[15] S. Kukreti, A. Cerussi, B. Tromberg, E. Gratton, *Dis. Markers* **2008**, *25*, 281–290.
[16] S. J. Matcher, et al., *Phys. Med. Biol.* **1994**, *39*, 177.
[17] J. J. Xia, E. P. Berg, J. W. Lee, G. Yao, *Meat Sci.* **2007**, *75*, 78–83.